INTERNATIONAL JOURNAL FOR NUMERICAL METHODS IN ENGINEERING
Int. J. Numer. Meth. Engng 2001; **50**:227–251

Dynamic modelling of the flat 2-D crack by a semi-analytic BIEM scheme

Taku Tada[1,*,†] and Raúl Madariaga[2]

[1]*Earthquake Research Institute, The University of Tokyo, 1-1-1 Yayoi, Bunkyo-ku, Tokyo 113-0032, Japan.*
[2]*Laboratoire de Géologie, École Normale Supérieure, 24, rue Lhomond, 75231 Paris Cedex 05, France*

SUMMARY

We present an efficient numerical method for solving indirect boundary integral equations that describe the dynamics of a flat two-dimensional (2-D) crack in all modes of fracture. The method is based on a piecewise-constant interpolation, both in space and time, of the slip-rate function, by which the original equation is reduced to a discrete convolution, in space and time, of the slip-rate and a set of analytically obtained coefficients. If the time-step interval is set sufficiently small with respect to the spatial grid size, the discrete equations decouple and can be solved explicitly. This semi-analytic scheme can be extended to the calculation of the wave field off the crack plane. A necessary condition for the numerical stability of this scheme is investigated by way of an exhaustive set of trial runs for a kinematic problem. For the case investigated, our scheme is very stable for a fairly wide range of control parameters in modes III and I, whereas, in mode II, it is unstable except for some limited ranges of the parameters. The use of Peirce and Siebrits' ε-scheme in time collocation is found helpful in stabilizing the numerical calculation. Our scheme also allows for variable time steps. Copyright © 2001 John Wiley & Sons, Ltd.

KEY WORDS: crack dynamics; boundary integral equation method; two-dimensional; numerical stability

1. INTRODUCTION

The boundary integral equation method (BIEM) has been extensively applied to various classes of dynamic crack-analysis problems [1]. According to the displacement discontinuity method using the indirect formulation, the traction on the crack surface is expressed as a convolution, in time and space, of the slip along the crack and a set of integration kernels. In the most straightforward form, these boundary integral equations (BIEs) are hypersingular and are not immediately amenable to numerical implementation. One of the most popular and successful methods to circumvent the hypersingularities is the approach of regularization, by which the integrals are rewritten, most often through integration by parts, in an equivalent form which involves only weakly singular integrals, at least integrable in the sense of Cauchy principal

*Correspondence to: Taku Tada, Earthquake Research Institute, The University of Tokyo, 1-1-1 Yayoi, Bunkyo-ku, Tokyo 113-0032, Japan
†E-mail: kogutek@eri.u-tokyo.ac.jp

Received 13 March 2000
Revised 20 September 2000

values. Although the formulation is possible both in the time domain and the frequency domain, the time-domain representation is preferable because it can deal not only with stationary but also with transient crack-analysis problems.

In conceptual terms, a time-domain formulation for the general non-planar three-dimensional (3-D) crack problem was first derived by Zhang [2], but it was not evident how it could be implemented to complicated problems. Theories more amenable to practical modelling were slower to appear. More recent modelling works, based on the displacement discontinuity method, the regularization technique and the time-domain representation, dealt with the flat two-dimensional (2-D) anti-plane crack [3, 4], flat 3-D crack [5–7], non-planar 2-D anti-plane and/or in-plane cracks [8–13], and the non-planar 3-D crack [14–16]. Meanwhile, an alternative formulation, based on a Fourier transform in space, was also developed [17–19].

While most of these works dealt with the behaviour of cracks placed in an infinite medium, Seelig and Gross [13] used a direct formulation so as to allow for cracks in finite media. They presented a set of advanced numerical simulations [12, 13], with rich implications for the interpretation of experimentally observed fracture phenomena [20].

The regularized BIEs, thus derived, may be reduced, by discretization, to a set of simultaneous linear algebraic equations, which have to be solved in a time-marching manner. The slip and traction profiles on the crack should then be approximated by linear combinations of a set of shape functions. If the crack is flat and if a temporally and spatially piecewise-constant approximation is used for the slip-rate function, the convolution coefficients in the discrete equations reduce to simple analytic forms [2, 3, 7, 15, 16]. If the discrete time-step interval is sufficiently small with respect to the spatial grid size, the simultaneous equations decouple and can be solved at each time step explicitly by simple summation [11, 21–23] further simplifying the computational scheme.

While this semi-analytic convolution method has already been elaborated for the flat 2-D anti-plane crack and the flat 3-D crack in previous works, in the present article we extend the theory to the flat 2-D in-plane crack. We also demonstrate that the same approach may be applied to the calculation of the wave field off the crack plane. We then investigate a necessary condition for the numerical stability of our time-marching BIEM scheme, both for 2-D anti-plane and in-plane motions, by an exhaustive set of experimental runs with different sets of control parameters. We also demonstrate that Peirce and Siebrits' ε-scheme [22] for time collocation enhances the stability of our numerical method under certain circumstances.

2. DEFINITION OF THE PROBLEM AND NOTATIONS

We assume that the medium is infinite, homogeneous and isotropic, and that the problem is independent of the x_3-axis; the crack, which is flat, lies on the x_1-axis. The slip components in the x_1-, x_2- and x_3-direction therefore correspond, respectively, to the in-plane shear mode (mode II), the opening mode (mode I), and the anti-plane shear mode (mode III).

In the present paper, $u_i(\mathbf{x},t)$ is the displacement in the ith direction at position $\mathbf{x}$ and time t, $\sigma_{ij}(\mathbf{x},t)$ the ij-component of the stress, Γ the crack surface, ξ or s the length co-ordinate along Γ, $\Delta u_i(\xi,\tau)$ the slip (or displacement discontinuity) on the crack in the ith direction at location ξ and time τ, $T_i(s,t)$ the traction along the crack surface in the ith direction

defined by

$$T_i(s,t) = \sigma_{ij}(s,t)n_j(s) \tag{1}$$

where $\mathbf{n}(s)$ is a unit vector normal to the crack surface, c_L and c_T the P- and S-wave velocity, respectively, μ the rigidity, a dot over a variable the derivative with time, $H(\cdot)$ the Heaviside step function, and

$$p \equiv c_T/c_L \tag{2}$$

The variable ξ or s, denoting the length co-ordinate along the crack, is taken equal to x_1. Greek subscripts stand for either 1 or 2. Summation over repeated indices is implied, wherever necessary.

The crack is supposed to lie initially in a uniform stress field σ^{ext}, while the traction $F(s)$ on the crack surface is defined by a separate boundary condition. For convenience, we take the stress at infinity as the zero reference state. This makes the problem equivalent to loading the crack, placed in a stress field that vanishes at infinity, with traction $T = F - \sigma^{\text{ext}}$.

3. BOUNDARY INTEGRAL EQUATIONS

3.1. *Anti-plane crack*

The BIE that defines the relation between the traction and slip on the surface of a flat 2-D anti-plane crack is [3]:

$$\begin{aligned} T_3(s,t) = &-\frac{\mu}{2\pi}\int_\Gamma \mathrm{d}\xi \frac{1}{s-\xi}\int_{-\infty}^{t} \mathrm{d}\tau \frac{\partial}{\partial \xi}\Delta\dot{u}_3(\xi,\tau)\frac{t-\tau}{\sqrt{(t-\tau)^2-((s-\xi)/c_T)^2}}H\left(t-\tau-\frac{|s-\xi|}{c_T}\right) \\ &-\frac{\mu}{2\pi}c_T^{-2}\int_\Gamma \mathrm{d}\xi \int_{-\infty}^{t} \mathrm{d}\tau \frac{\partial}{\partial \tau}\Delta\dot{u}_3(\xi,\tau)\frac{1}{\sqrt{(t-\tau)^2-((s-\xi)/c_T)^2}}H\left(t-\tau-\frac{|s-\xi|}{c_T}\right) \end{aligned} \tag{3}$$

We apply a temporally and spatially piecewise-constant interpolation to the slip rate [3, 7, 10, 15, 16]:

$$\Delta\dot{u}_3(s,t) = \sum_{k,m} D_3^{k,m} d^{k,m}(s,t) \tag{4}$$

$$d^{k,m}(s,t) \equiv \left[H(s-s_k+\tfrac{1}{2}\Delta s) - H\left(s-s_k-\tfrac{1}{2}\Delta s\right)\right]\cdot\left[H\left(t-t_m^{\text{short}}\right) - H\left(t-t_m^{\text{long}}\right)\right] \tag{5}$$

$$t_m^{\text{short}} \equiv t_m - e_t\Delta t_m, \quad t_m^{\text{long}} \equiv t_m + (1-e_t)\Delta t_m, \quad 0 < e_t \leqslant 1 \tag{6}$$

The spatial grid size Δs is taken to be uniform all over the fault, in order to assure space-translation invariance of the discrete formulation. The time-step interval Δt_m is usually taken to be constant also for the sake of time-translation invariance, but in the present study, we leave room for variable time-step intervals. The parameter e_t stands for the relative height

of the time collocation point t_m within the time-step interval Δt_m; $e_t = 1$ if variables are collocated at the end of the interval and $e_t = 0.5$ if they are collocated at the midpoint. Some authors [2, 5, 11–13], who employed the same interpolation method, used special square-root-type shape functions for the crack-end elements, which we did not. The discretization reduces the original integral equation to

$$T_3^{i,n} \equiv T_3(s_i, t_n) = -\frac{\mu}{2c_T} \sum_{k,m} D_3^{k,m} K_{3:T3}^{i-k,n,m} \tag{7}$$

with [3]

$$\begin{aligned} K_{3:T3}^{i-k,n,m} \equiv\ & I_{3:T3}\left(\left(i-k+\tfrac{1}{2}\right)\Delta s, t_n - t_m^{\text{short}}\right) - I_{3:T3}\left(\left(i-k-\tfrac{1}{2}\right)\Delta s, t_n - t_m^{\text{short}}\right) \\ & - I_{3:T3}\left(\left(i-k+\tfrac{1}{2}\right)\Delta s, t_n - t_m^{\text{long}}\right) + I_{3:T3}\left(\left(i-k-\tfrac{1}{2}\right)\Delta s, t_n - t_m^{\text{long}}\right) \end{aligned} \tag{8}$$

$$\begin{aligned} I_{3:T3}(s,t) =\ & \frac{c_T}{\pi s} H(t) \int_0^t \mathrm{d}\tau \frac{\tau}{\sqrt{\tau^2 - (s/c_T)^2}} H\left(\tau - \frac{|s|}{c_T}\right) + \frac{1}{\pi c_T} H(t) \\ & \times \int_{-\infty}^{s} \mathrm{d}\xi \frac{1}{\sqrt{t^2 - (\xi/c_T)^2}} H\left(t - \frac{|\xi|}{c_T}\right) \\ =\ & H(s)H(t) + \frac{1}{\pi}\ \mathrm{sgn}(s) H\left(t - \frac{|s|}{c_T}\right)\left[\sqrt{(c_T t/s)^2 - 1} - \mathrm{Arccos}\frac{|s|}{c_T t}\right] \end{aligned} \tag{9}$$

Cochard and Madariaga [3, Equation (8)] derived an alternative equation to Equation (3), in which the radiation damping term $-(\mu/(2c_T))\Delta\dot{u}_3(s,t)$ was isolated from the rest of the equation. However, the use of their alternative formula results in a discrete equation with the same coefficients (9).

3.2. *In-plane crack*

The BIEs for the tangential and normal tractions on the in-plane crack are given by [10]

$$\begin{aligned} T_1(s,t) =\ & -\frac{2\mu}{\pi} c_T^2 \int_\Gamma \mathrm{d}\xi \frac{1}{(s-\xi)^3} \int_{-\infty}^{t} \mathrm{d}\tau \frac{\partial}{\partial \xi} \Delta\dot{u}_1(\xi,\tau) \\ & \times \left[(t-\tau)\sqrt{(t-\tau)^2 - ((s-\xi)/c_L)^2} H\left(t - \tau - \frac{|s-\xi|}{c_L}\right)\right. \\ & \left. - (t-\tau)\sqrt{(t-\tau)^2 - ((s-\xi)/c_T)^2} H\left(t - \tau - \frac{|s-\xi|}{c_T}\right)\right] \\ & - \frac{\mu}{2\pi} c_T^{-2} \int_\Gamma \mathrm{d}\xi \int_{-\infty}^{t} \mathrm{d}\tau \frac{\partial}{\partial \tau} \Delta\dot{u}_1(\xi,\tau) \\ & \times \frac{1}{\sqrt{(t-\tau)^2 - ((s-\xi)/c_T)^2}} H\left(t - \tau - \frac{|s-\xi|}{c_T}\right) \end{aligned} \tag{10}$$

$$T_2(s,t)=\frac{2\mu}{\pi}c_T^2\int_\Gamma \mathrm{d}\xi\frac{1}{(s-\xi)^3}\int_{-\infty}^{t}\mathrm{d}\tau\frac{\partial}{\partial\xi}\Delta\dot{u}_2(\xi,\tau)$$
$$\times\left[(t-\tau)\sqrt{(t-\tau)^2-((s-\xi)/c_L)^2}H\left(t-\tau-\frac{|s-\xi|}{c_L}\right)\right.$$
$$\left.-(t-\tau)\sqrt{(t-\tau)^2-((s-\xi)/c_T)^2}H\left(t-\tau-\frac{|s-\xi|}{c_T}\right)\right]$$
$$-\frac{2\mu}{\pi}(1-p^2)\int_\Gamma \mathrm{d}\xi\frac{1}{s-\xi}\int_{-\infty}^{t}\mathrm{d}\tau\frac{\partial}{\partial\xi}\Delta\dot{u}_2(\xi,\tau)\frac{t-\tau}{\sqrt{(t-\tau)^2-((s-\xi)/c_L)^2}}$$
$$\times H\left(t-\tau-\frac{|s-\xi|}{c_L}\right)-\frac{\mu}{2\pi}c_T^{-2}\int_\Gamma \mathrm{d}\xi\int_{-\infty}^{t}\mathrm{d}\tau\frac{\partial}{\partial\tau}\Delta\dot{u}_2(\xi,\tau)$$
$$\times\frac{1}{\sqrt{(t-\tau)^2-((s-\xi)/c_L)^2}}H\left(t-\tau-\frac{|s-\xi|}{c_L}\right) \tag{11}$$

With the piecewise-constant interpolation of the slip-rate

$$\Delta\dot{u}_1(s,t)=\sum_{k,m}D_1^{k,m}d^{k,m}(s,t) \tag{12}$$

$$\Delta\dot{u}_2(s,t)=\sum_{k,m}D_2^{k,m}d^{k,m}(s,t) \tag{13}$$

they reduce to

$$T_1^{i,n}\equiv T_1(s_i,t_n)=-\frac{\mu}{2c_T}\sum_{k,m}D_1^{k,m}K_{1:T1}^{i-k,n,m} \tag{14}$$

$$T_2^{i,n}\equiv T_2(s_i,t_n)=-\frac{\mu}{2c_T}\sum_{k,m}D_2^{k,m}K_{2:T2}^{i-k,n,m} \tag{15}$$

with

$$K_{1:T1}^{i-k,n,m}=I_{1:T1}\left(\left(i-k+\tfrac{1}{2}\right)\Delta s,t_n-t_m^{\text{short}}\right)-I_{1:T1}\left(\left(i-k-\tfrac{1}{2}\right)\Delta s,t_n-t_m^{\text{short}}\right)$$
$$-I_{1:T1}\left(\left(i-k+\tfrac{1}{2}\right)\Delta s,t_n-t_m^{\text{long}}\right)+I_{1:T1}\left(\left(i-k-\tfrac{1}{2}\right)\Delta s,t_n-t_m^{\text{long}}\right) \tag{16}$$

and likewise for $K_{2:T2}$, and

$$I_{1:T1}(s,t)=H(s)H(t)+\frac{1}{\pi}\mathrm{sgn}(s)H\left(t-\frac{|s|}{c_L}\right)\frac{4}{3}p^3\left[(c_Lt/s)^2-1\right]^{3/2}$$
$$-\frac{1}{\pi}\mathrm{sgn}(s)H\left(t-\frac{|s|}{c_T}\right)\left\{\frac{4}{3}\left[(c_Tt/s)^2-1\right]^{3/2}+\mathrm{Arccos}\frac{|s|}{c_Tt}\right\} \tag{17}$$

$$I_{2:T2}(s,t)=\frac{1}{p}H(s)H(t)+\frac{1}{\pi}\mathrm{sgn}(s)H\left(t-\frac{|s|}{c_L}\right)\left\{-\frac{4}{3}p^3\left[(c_Lt/s)^2-1\right]^{3/2}+4p(1-p^2)\right.$$
$$\left.\times\sqrt{(c_Lt/s)^2-1}-\frac{1}{p}\mathrm{Arccos}\frac{|s|}{c_Lt}\right\}+\frac{1}{\pi}\mathrm{sgn}(s)H\left(t-\frac{|s|}{c_T}\right)\frac{4}{3}\left[(c_Tt/s)^2-1\right]^{3/2} \tag{18}$$

3.3. Friction laws

In order to solve Equations (7), (14) or (15), we have to combine them with a boundary condition, in the form of a friction law, that defines the relation between the traction T and the slip-rate $\Delta\dot{u}$ (or D) on the crack surface. A simplest example is the friction-free condition

$$T+\sigma^{\mathrm{ext}}=0 \tag{19}$$

where the external stress σ^{ext} has been subtracted from our definition of the traction T so that the latter may equal zero at infinity.

Alternatively, it is possible to employ other types of friction laws, including the triangular slip-weakening law [24]

$$T+\sigma^{\mathrm{ext}}=\begin{cases}\sigma_0(1-\Delta u/D_0) & (0<\Delta u<D_0)\\ 0 & (D_0\leqslant\Delta u)\end{cases} \tag{20}$$

which will be used later in our article. The specific form of Equation (20) has the advantage of allowing the slip-rate D to be solved for explicitly in an analytical form.

When modelling spontaneous evolution of the crack, we employed the critical-stress rupture criterion, according to which the crack tip is made to advance if and only if the traction on the node next to the crack end has exceeded a certain threshold value. Strictly speaking, this criterion is dependent on the discretization. When the spatial grid size is fixed, however, the critical-stress criterion is approximately equivalent to the stress intensity factor-based criterion that is derived from fracture energy considerations, as long as the rupture speed is not too large [25]. Otherwise, an energy-based criterion should be used in our numerical method. This limitation of the critical-stress criterion does not affect the results presented here, however, since they have to do with the long-term stability behaviour of the BIEM time-marching scheme.

3.4. Implicit and explicit regimes

In general, the discretized BIE (7), (14) or (15), together with the friction law, must be solved in an implicit way as a set of simultaneous linear algebraic equations. If the ratio of the time-step size to the spatial grid size is small enough, however, these simultaneous equations decouple and reduce to an explicit formulation [11, 21–23]. Let

$$h_T\equiv c_T\,\Delta t/\Delta s,\quad h_L\equiv c_L\,\Delta t/\Delta s \tag{21}$$

be the Courant–Friedrichs–Lewy (CFL) parameter, and if

$$e_t h_T \leqslant \tfrac{1}{2} \tag{22}$$

in the anti-plane mode, or

$$e_t h_L \leqslant \tfrac{1}{2} \quad \text{or} \quad e_t h_T \leqslant p/2 \tag{23}$$

in the in-plane modes, the elastic field at the collocation point (s_i, t_n) lies outside the cone of influence (or of causality) of the elastic waves emitted from the neighbouring contemporaneous blocks collocated at (s_{i+1}, t_n) and (s_{i-1}, t_n). This decouples Equations (7), (14) or (15) and reduces them to

$$T_3^{i,n} = -\frac{\mu}{2c_T}\left(D_3^{i,n} + \sum_{k,m<n} D_3^{k,m} K_{3:T3}^{i-k,n,m}\right) \tag{24}$$

$$T_1^{i,n} = -\frac{\mu}{2c_T}\left(D_1^{i,n} + \sum_{k,m<n} D_1^{k,m} K_{1:T1}^{i-k,n,m}\right) \tag{25}$$

$$T_2^{i,n} = -\frac{\mu}{2c_T}\left(\frac{1}{p} D_2^{i,n} + \sum_{k,m<n} D_2^{k,m} K_{2:T2}^{i-k,n,m}\right) \tag{26}$$

This allows the slip-rate D to be solved for explicitly by simple summation. The explicit formulation was used in a number of earlier publications [3, 4, 7, 16], but the authors were not clearly aware of the role of the CFL parameter in the BIEM.

3.5. *Some technical notes*

The spatio-temporal convolution of the form $\sum_{k,m<n} D^{k,m} K^{i-k,n,m}$ should better be calculated by way of Fast Fourier Transform (FFT) in space, because this reduces the computational costs significantly [4, 26]. However, FFT cannot be applied to the summation in time under the time-marching scheme.

A remark should also be made on the accuracy of computation for the convolution coefficients. In the in-plane problem, $I_{1:T1}$ and $I_{2:T2}$ may become highly inaccurate for $c_T t/s \gg 1$ if they are calculated according to Equations (17) and (18), because they contain a difference between two large values. In order to preclude round-off errors, it is advisable, for $c_L t/s \gg 1$, to approximate $I_{1:T1}$ and $I_{2:T2}$ by their asymptotes

$$I_{1:T1}^{st}(s,t) = I_{2:T2}^{st}(s,t) \equiv \frac{2c_T t}{\pi s}(1 - p^2) \tag{27}$$

since the convergence to these asymptotes is fairly rapid. Although the inaccuracy problem is not evident in the anti-plane mode, a similar approximation is possible if we replace $I_{3:T3}$ by

its asymptote

$$I^{st}_{3:T3}(s,t) \equiv \frac{c_T t}{\pi s} \tag{28}$$

for $c_T t/s \gg 1$.

4. OFF-FAULT ELASTIC FIELD

The same discretization can be adapted to the off-fault stress and displacement field. If we discretize Tada and Yamashita's [10] Equations (B1), (B2), (B8) and (B9), adapted to the special case of a flat crack, with the piecewise-constant interpolations (4), (12) and (13) of the slip-rate, we obtain

$$\sigma^{i,j,n}_{3\alpha} \equiv \sigma_{3\alpha}(x^i_1, x^j_2, t_n) = -\frac{\mu}{2c_T}\sum_{k,m} D^{k,m}_3 K^{i,j,k,n,m}_{3:\sigma 3\alpha} \tag{29}$$

$$\sigma^{i,j,n}_{\alpha\beta} \equiv \sigma_{\alpha\beta}(x^i_1, x^j_2, t_n) = -\frac{\mu}{2c_T}\sum_{k,m} \left[D^{k,m}_1 K^{i,j,k,n,m}_{1:\sigma\alpha\beta} + D^{k,m}_2 K^{i,j,k,n,m}_{2:\sigma\alpha\beta}\right] \tag{30}$$

$$u^{i,j,n}_3 \equiv u_3(x^i_1, x^j_2, t_n) = \sum_{k,m} D^{k,m}_3 K^{i,j,k,n,m}_{3:u3} \tag{31}$$

$$u^{i,j,n}_\alpha \equiv u_\alpha(x^i_1, x^j_2, t_n) = \sum_{k,m} \left[D^{k,m}_1 K^{i,j,k,n,m}_{1:u\alpha} + D^{k,m}_2 K^{i,j,k,n,m}_{2:u\alpha}\right] \tag{32}$$

where the convolution coefficients are given in the appendix.

5. BASIC NUMERICAL EXAMPLES

5.1. *Self-similar fault evolution*

Our theory allows us to simulate the dynamics of a flat 2-D crack in an efficient way. First, we illustrate the performance of our modelling scheme using a self-similarly evolving fault model. In all the numerical examples that follow, we assumed $p = 1/\sqrt{3}$ or $c_L = \sqrt{3}c_T$, as is commonly done. Also, the time-step interval Δt was held constant throughout a numerical run, unless otherwise stated.

We modelled the kinematic evolution of a planar fault, 309 grids long, which begins to break at its midpoint at the initial time step and propagates bilaterally at a fixed speed of 0.9 times the Rayleigh wave speed $c_R = 0.919c_T$. This propagation speed is equal to that in the mode II numerical test presented by Andrews and Ben-Zion [27, Appendix]. We set the other parameters equal to theirs: $\Delta s = 0.025$, $c_T = 1.0$ and $\mu = 1.0$, and no friction was assumed on the crack surface. As in their paper, we present the calculated stress and traction so that the uniform external stress level is equal to 1.0 and the stress drop on the broken patch of the fault is equal to 0.5. This is different from the definition used elsewhere in the present paper in which the external stress level is taken as the zero reference state. Further, as in their

example, the traction on the crack was made to vary linearly at the ends, so that it takes two spatial grid intervals for it to drop from 1.0 to 0.5. No artificial damping was used.

Figures 1 and 2 show the numerical results in terms of the time evolution of the slip, slip-rate and traction on the crack, as well as the stress and displacement-rate field off the fault

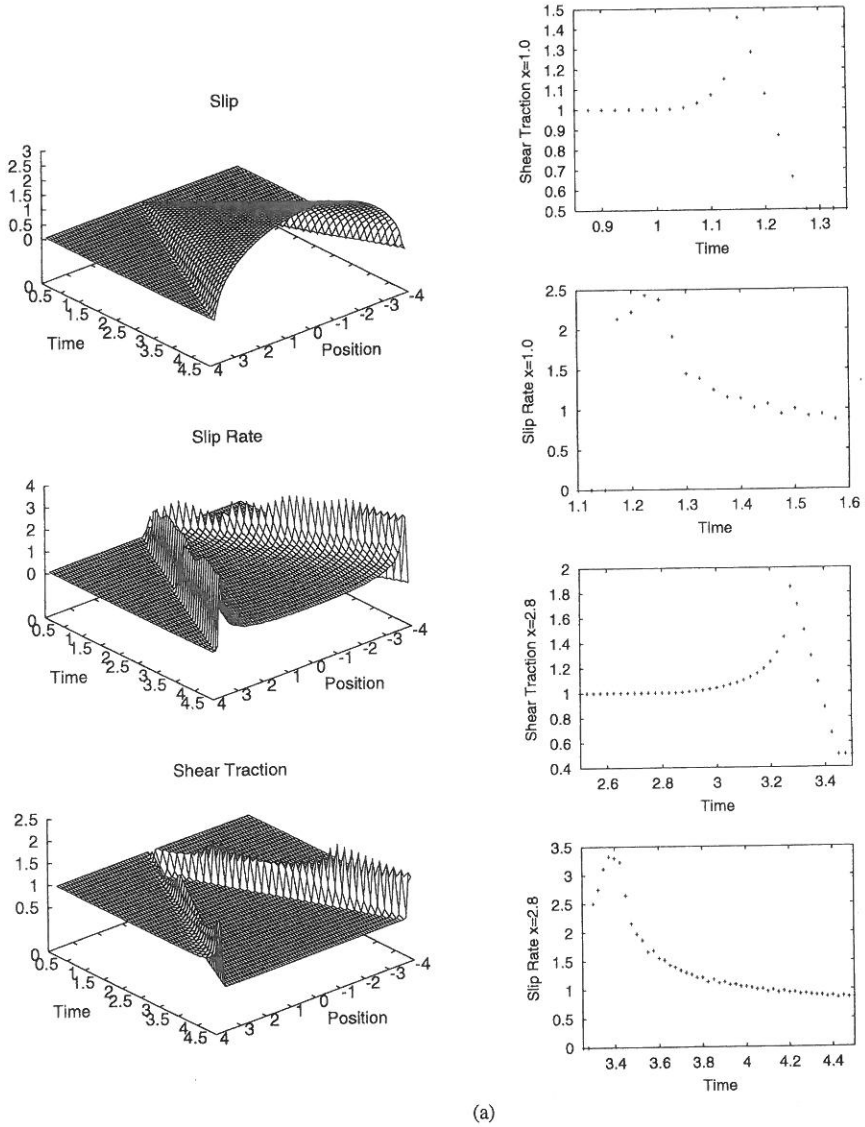

(a)

Figure 1. Self-similarly evolving planar 2-D crack in mode III, with $h_T = 1.0$ and $e_t = 0.43$, over 180 time steps: (a) Left, time evolution of the traction, slip-rate and slip on the fault. Right, time variation of the traction and slip-rate at fixed points: top, traction at location 1.0 from the midpoint; second, slip-rate at location 1.0; third, traction at location 2.8; bottom, slip-rate at location 2.8; (b) Off-fault elastic field at the 60th time step or time 1.5. Top and middle, stress components σ_{31} and σ_{32}; bottom, displacement-rate component $\dot{u}_3$.

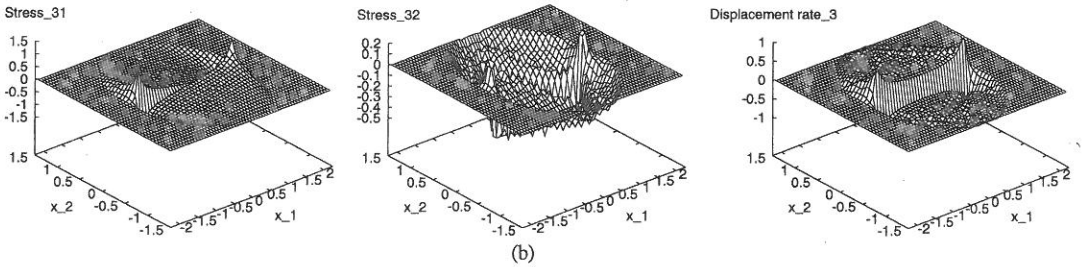

(b)

Figure 1. *Continued.*

plane, for modes II and III; similar figures for mode I are omitted for brevity. The control parameters were $h_T = 1.0$ and $e_t = 0.43$ for mode III and $h_T = 0.5$ and $e_t = 1.0$ for mode II; as shown in the next section, these assure numerical stability. It is worth noting in these figures that, even though the calculated slip has a smooth profile on the crack, the off-fault elastic field appears fairly noisy, presumably due to the intermittent advancement of the crack tip along the discretized model fault. This hypothesis on the origin of the noise comes from the observation that, when we prescribed a slip-weakening friction law on the crack surface so that the onset of slip might be smoother, the ragged off-fault field profile tended to smooth too. However, since the off-fault field is no input to the BIE scheme, noise therein has no harmful effects on the stability of the numerical scheme.

The time variation plots for the traction and slip-rate at two fixed locations, appearing in these figures, are directly comparable to equivalent plots for mode II appearing in Reference [27] as Figures A1–A4 (reproduced in solid lines on the right-hand-side panels of Figure 2a). Since, in their results, the calculated time variations were noisier and much less stable for the BIEM calculation than for the finite difference method (FDM), they argued that the FDM was superior to the BIEM as a method for fault dynamics modelling. However, they used an indirect BIE that corresponds to the inverse of the formulation in our present study. In our modelling, the time variation profiles were smoother than their FDM results, as is visible in our Figure 2a (though for the combination $h_T = 0.25$ and $e_t = 1.0$, the profiles were just as smooth as theirs, and for $h_T = 0.5$ and $e_t = 0.3$, they were less smooth). This implies that the BIEM can be as effective as the FDM, contrary to Andrews and Ben-Zion's conclusion.

5.2. *Spontaneous fault evolution*

Next, we illustrate the numerical result for a spontaneously evolving planar fault. Using the same parameters as in the foregoing section for Δs, c_T and μ, we made a 31-grid-long crack in mode III which abruptly emerge at the midpoint of a 309-grid-long planar fault, and traced its spontaneous evolution according to the critical-stress rupture criterion. Figure 3 shows the result of the calculation with control parameters $h_T = 1.0$ and $e_t = 0.43$. The external stress σ^{ext} was set at 0.5, the critical stress T_u at 1.0, and the friction law parameters in (20) were $\sigma_0 = 0.495$ and $D_0 = 0.3$. This satisfies the condition recommended for the accurate resolution of the slip-rate near the rupture front [28]:

$$D_0 > 4 \cdot 2T_u \Delta s/\mu \tag{33}$$

No artificial damping was used. We suppressed back-slipping: wherever a negative slip-rate was expected, we temporarily locked that part of the fault. The asymmetry in the figure is due to data decimation in drawing.

Compared with the kinematic modelling result shown in Figure 1a, we see that the slip-rate and traction outputs are more prone to fluctuation and occasional emergence of extraordinarily large values (some of which have been clipped off in the slip-rate graph for a clearer display of the other parts).

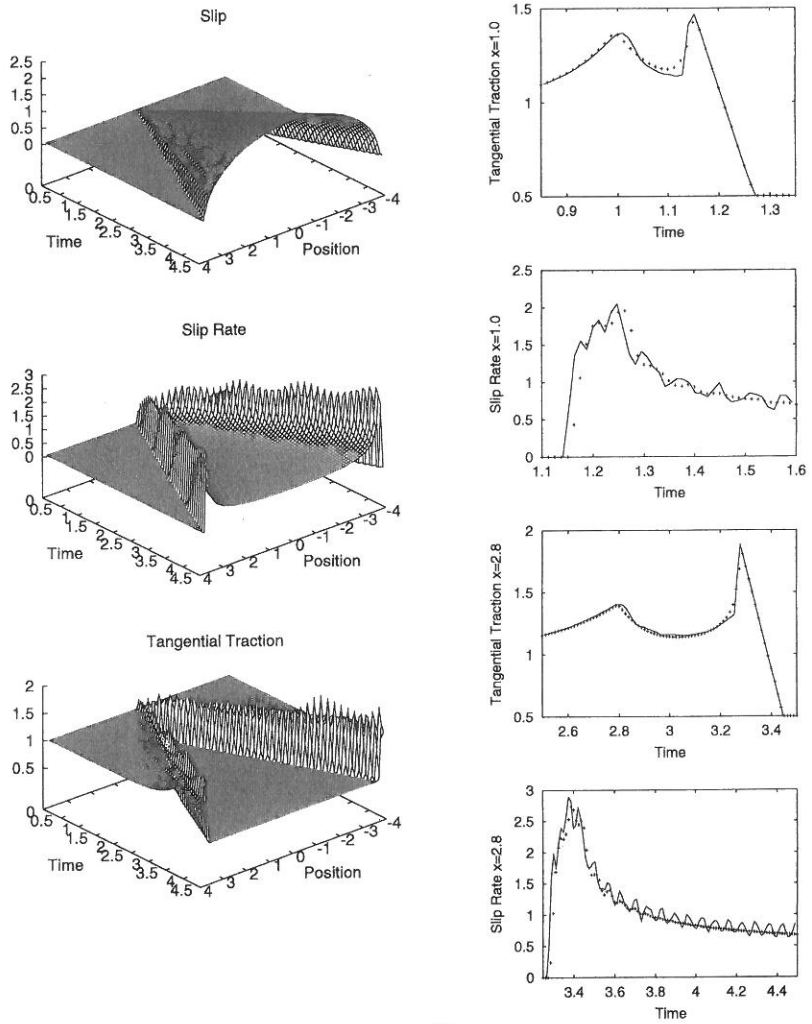

(a)

Figure 2. Self-similar mode II crack, with $h_T = 0.5$ and $e_t = 1.0$, over 360 time steps: (a) Traction, slip-rate and slip profiles. Legends as in Figure 1a. The solid lines in the panels on the right-hand side are corresponding FDM results by Andrews and Ben-Zion [27]; (b) Off-fault elastic field at the 60th time step or time 0.75. Top left, middle left and bottom left, stress components σ_{12}, σ_{11} and σ_{22}; top right and middle right, displacement-rate components $\dot{u}_1$ and $\dot{u}_2$.

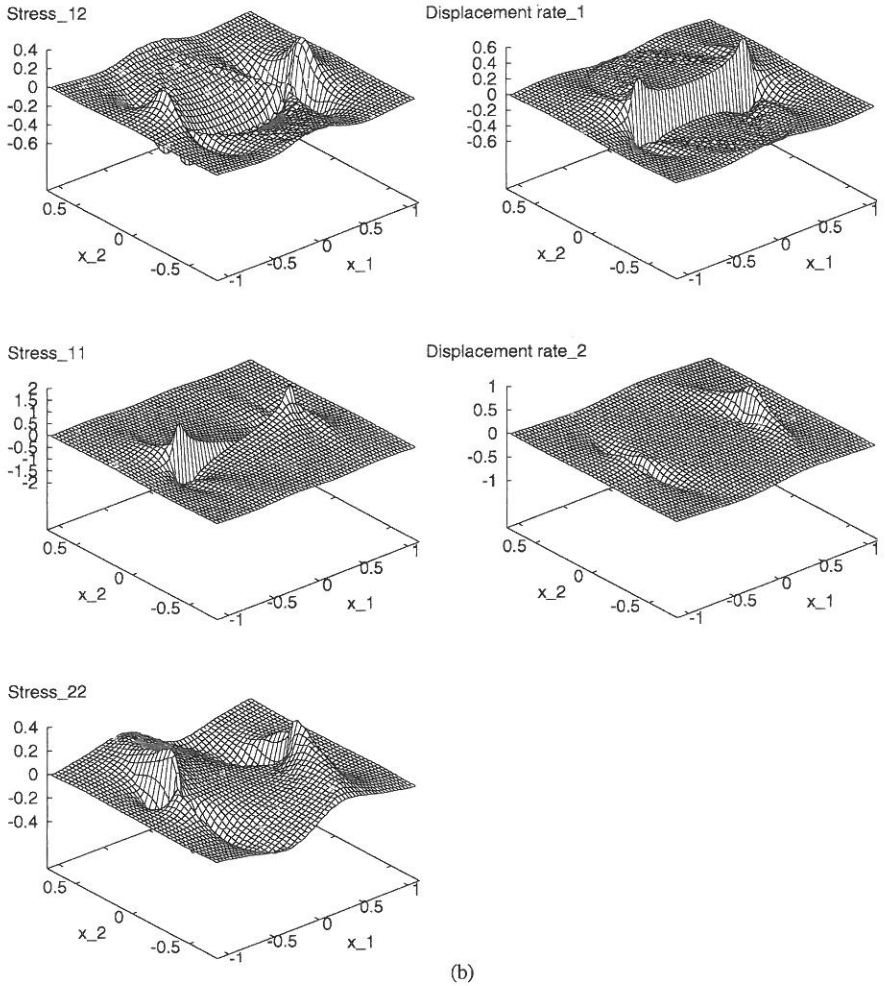

(b)

Figure 2. *Continued.*

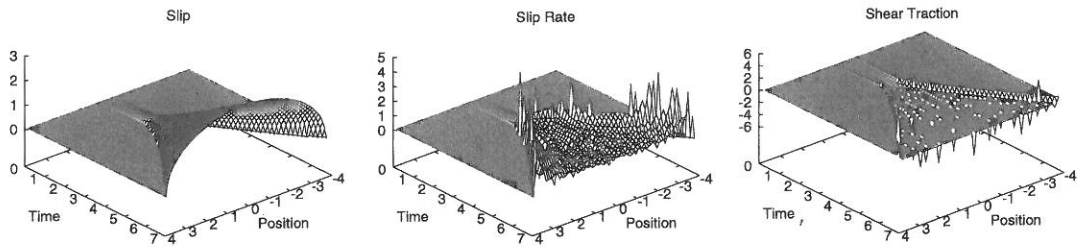

Figure 3. Spontaneously evolving mode III crack, with $h_T = 1.0$ and $e_t = 0.43$, over 277 time steps. Legends as in Figures 1a.

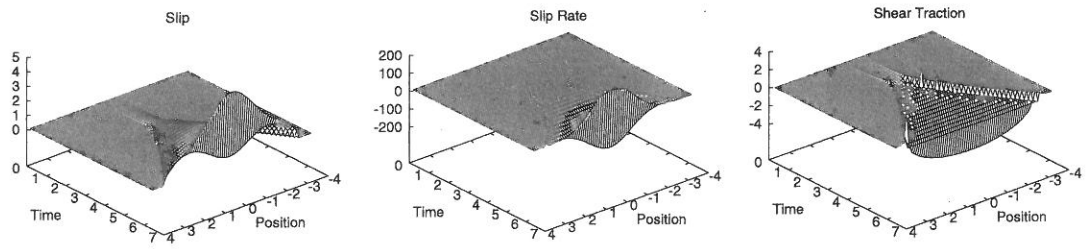

Figure 4. Spontaneously evolving mode III crack, with $h_T = 1.0$ and $e_t = 0.45$, over 251 time steps. Legends as in Figures 1a. Numerical instability is observed.

6. NUMERICAL STABILITY

The stability of our BIEM numerical scheme depends on the choice of the grid parameter h and the time collocation parameter e_t. For a wrong choice of these, oscillatory noise starts to develop in the solution, amplifies and eventually explodes. We have found out, as shown below, that the determination of the optimal pair (h, e_t) is in fact more complicated a problem than was envisaged by many previous authors. Figure 4 shows an example of the numerical instability, in which we simulated the spontaneous evolution of a mode III crack under the same conditions as in Figure 3, except that we used control parameters $h_T = 1.0$ and $e_t = 0.45$ and that we tolerated back-slipping.

The origin and nature of the instability phenomenon in the BIEM (both direct and indirect) time-marching scheme [29, 30] are not very well known. Some authors, in their modelling of the 2-D or 3-D crack, found their scheme unstable and suppressed the oscillation build-up by introducing an artificial dissipation term [8, 10] or by introducing a slip-weakening friction law [7, 26]. These methods did help to delay the manifestation of unstable oscillations but did not provide a fundamental remedy; this implies that the instabilities are not due to the inadequate modelling of the rupture phenomenon, since the oscillations persisted even when appropriate account was taken of the finite length scale, an essential feature of the fault constitutive laws [31]. Others [2–4] found their BIEM time-marching scheme very stable even after a long numerical run in the modelling of the flat 2-D anti-plane crack. As Peirce and Siebrits pointed out [22, 23], the instabilities are elusive in nature since they tend to appear intermittently as the grid parameter h is changed continually.

Koller *et al.* [8] pointed out the spatial, not temporal, nature of the unstable oscillations in an indirect BIEM. Frangi and Novati [32] and Frangi [33, 34], who used a direct BIEM formulation, also reflected on their origin using simple model cases, and argued that the failure of the conventional interpolation method to accurately simulate the continuous propagation of wave fronts and to respect the causality condition was one of the sources of the instabilities. A more general mathematical approach to the problem of convergence and stability of a discretized BIE was provided by Lubich [35]. However, Peirce and Siebrits [22, 23] were the first to provide a theoretically consistent framework to this question; their work, using the z-transform, suggested that the calculation could be absolutely stable for certain numerical schemes and control parameters. They also pointed out that the numerical scheme was more likely to be stable if the 'self-effect', or the influence a grid element or collocation point has on itself with no time delay ($K^{0,n,n}$ in our terminology), was larger than the other

element-to-element effects. Birgisson *et al.* [36], who dealt with direct BIEs, speculated that the instabilities could also be due to numerical inaccuracies in treating a wave front cutting partially through a discrete element and in evaluating element-to-element effects with large time delays.

In the BIEM, there are no intrinsic limits on the value of the grid parameter h, except that the solution regime is explicit only when $e_t h \leqslant \frac{1}{2}$ (we call this the CFL limit in analogy to the FDM). To cover a given time duration with a minimal number of time steps, larger values of h are preferable, whereas smaller values of h are preferred for a finer time resolution. Meanwhile, small values of h are prone to oscillatory numerical instabilities [7, 9, 11, 30, 32, 33]. Cochard and Madariaga [3, 4] fixed h_T at 0.5 and found out empirically that $e_t = 1.0$ gave the best and most stable result for the planar 2-D anti-plane crack. Fukuyama and Madariaga [7] fixed e_t at 1.0 and decided, by trial and error, that $h_T = 0.5$ gave the optimal result for the 3-D quasi-anti-plane crack, and $h_T = 0.25$ for the 3-D circular crack. Seelig and Gross [11], who used a scheme equivalent to $e_t = 1.0$, recommended the range $0.5 \leqslant h_L \leqslant 1.0$ for the non-planar 2-D in-plane crack.

In order to study the instability, we carried out an exhaustive set of experimental numerical runs for different sets of control parameters (h_T, e_t) in all three modes of fracture. The model crack was made to grow self-similarly, with a fixed speed of $0.9c_R$, from the midpoint of a fault composed of 49 space grids, and, after the crack ends have reached the ends of the fault, the calculation was continued with a stationary crack geometry. An abrupt stress drop was assumed at the tips of the crack, on which no friction was assumed and back-slipping was tolerated. We measured the degree of instability in terms of the number of time steps elapsed before the amplitude of the oscillation exceeded a certain threshold level. The amplitude was measured by the maximum absolute value of the calculated slip, and the threshold was equal to 8.2 times the final elastostatic midfault slip in the anti-plane mode and 10.9 times that in the in-plane modes. We ran the time-marching scheme over 1000 time steps, and if the above instability criterion was not reached by the 1000th time step, we looked at the final slip profile, and, if the calculated slip decreased monotonously from the midpoint to the ends, we labeled it as 'very stable', and otherwise, we termed it as 'near-stable'. We plotted, in Figures 5–7, the map of this instability indicator in the parameter space h_T–e_t.

In interpreting the experimental results, it should be realized that our experiments do not guarantee that the stability behaviour will be the same for any crack evolution history. In this sense, our results should be regarded as providing a necessary condition for the stability. However, Peirce and Siebrits' theory [22, 23] suggests that the stability does not, in principle, depend on specific slip histories. In fact, the results changed very little when we used a crack propagation velocity of $0.5c_R$, or when crack propagation was initiated from a finite length instead of a single point.

The 'very stable' and 'near-stable' labels should be taken with caution. In fact, we sometimes saw these two labels replaced by each other when we carried out the numerical calculation under different slip histories as stated above. The 'very stable' label does not automatically guarantee that the scheme is going to remain stable as long as you like. We consider, however, that the 'stable/unstable' labelling represents, for practical purposes, a good enough indicator of the long-term stability behaviour of the BIEM scheme.

Imposing a gradual stress drop on the crack ends [27] had the effect of only marginally delaying the instability build-up. This implies that the presence of a length scale in the formulation, which is essential in modelling a spontaneously evolving crack [31], does not

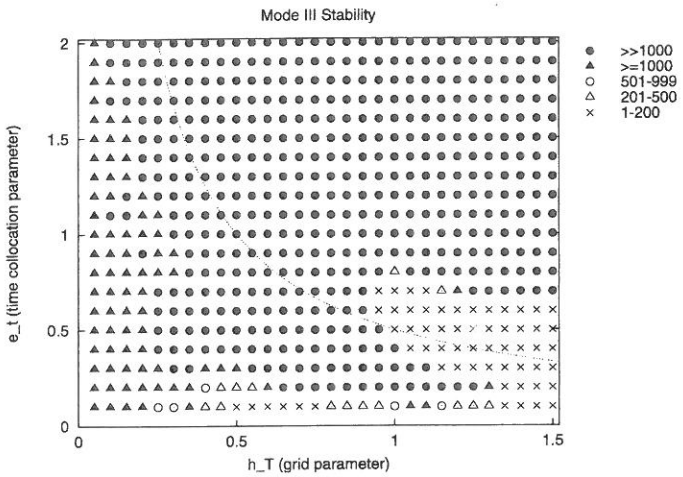

Figure 5. Stability map in mode III for different sets of control parameters h_T and e_t, for a kinematic model of a bilaterally propagating crack. Filled circles stand for high stability, filled triangles for near-stability, while open circles, open triangles and X's stand for instability. The broken curve is the CFL limit, above and to the right of which the BIE should be solved implicitly. For $e_t > 1$, Peirce and Siebrits' ε-scheme is used.

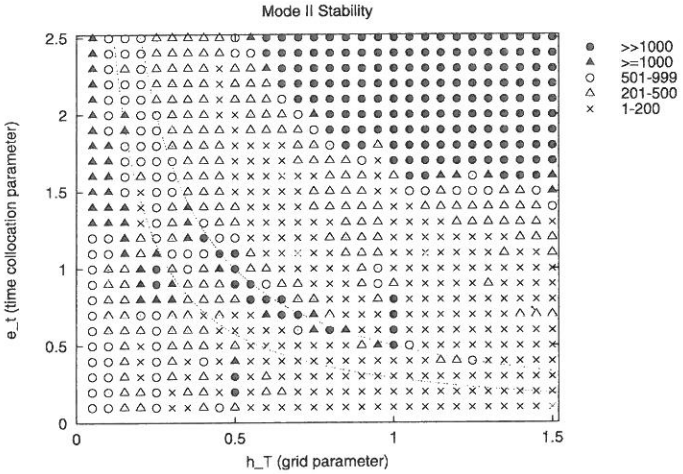

Figure 6. Stability map in mode II. Legends as in Figure 5. The two broken curves are the CFL limits for the P and S waves.

necessarily play a major role in the stabilization of the numerical scheme, at least in the case investigated here.

As we can see in Figures 5–7, the scheme proved stable, when $e_t \leqslant 1$, for a fairly wide range of control parameters in modes I and III; in mode II, it was unstable over most part of the parameter plane. Curiously, there are at least four isolated islands of stability in mode II, namely, near $h_T = 0.25$ and $e_t = 0.9$–1.0, $h_T = 0.5$ and $e_t = 0.2$–0.3, $h_T = 1.0$ and $e_t = 0.5$–0.8,

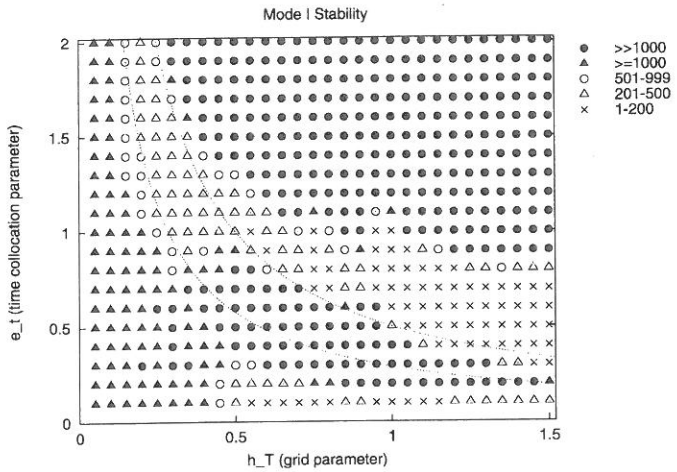

Figure 7. Stability map in mode I. Legends as in Figures 5 and 6.

and along the curve $h_T \cdot e_t = 0.5$; the first one was discovered by Cochard (1998, pers. comm.). This suggests that the numerical instability of the BIEM scheme, pointed out by so many authors, may, in fact, not be intrinsic to the scheme but depend on the choice of the control parameters. The mode II result well illustrates the intermittent appearance of instabilities with changing h [22, 23]. When we allow h and e_t to change independently, however, we see that the pattern of instability emergence is still more complicated.

In Figures 5–7, we also mapped the case of $e_t > 1$. Peirce and Siebrits [22] pointed out that such a measure tended to improve the stability of a BIEM scheme, because it enhanced the 'self-effect' ($K^{0,n,n}$) while the other element-to-element effects remained largely unaltered, and called this method the 'ε-scheme' (their parameter ε corresponds to $e_t - 1$ in our terminology). Definitions (5) and (6) remain the same, except that, when dealing with the nth time step, the contemporaneous time-step interval Δt_n is extended up to t_n, so that (Figure 8)

$$t_n^{\text{short}} \equiv t_n - e_t \Delta t_n, \quad t_n^{\text{long}} \equiv t_n, \quad e_t > 1 \tag{34}$$

As seen in Figure 6, we found out that the modes I and II calculations were very stable over a wide range of h_T if we took e_t larger than about 1.2 and 1.6, respectively. The calculation results were accurate and smooth, although a certain time delay was duly recognized (Figure 9). The BIEM scheme was also very stable in mode III for $e_t > 1$ except for very small values of h_T. This agrees with Peirce and Siebrits' argument [22, 23] that the ε-scheme helps to enhance numerical stability.

As for the cause of the numerical instabilities, we found out that the unstable region, found in the lower right part of Figure 5 roughly for $h_T > 0.9$ and $e_t < 0.7$, approximately coincided with the region where the self-effect $K^{0,n,n}$ was smaller than the delayed effect $K^{1,n,n}$, which is in line with Peirce and Siebrits' speculations [22, 23]. Otherwise, however, no obvious relationship was found out between the instability of the BIEM scheme and the relative magnitude of the self-effect with regard to other element-to-element effects.

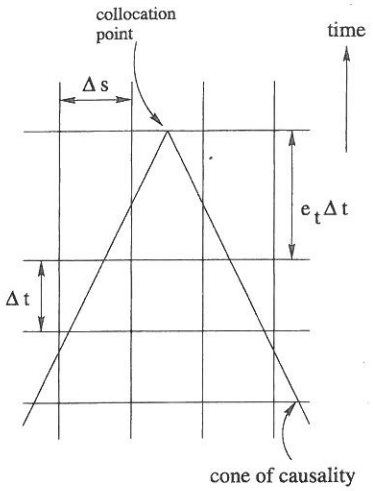

Figure 8. Peirce and Siebrits' ε-scheme.

It is worth noting that the similar BIEM scheme for the planar 3-D shear crack is unstable for the set $e_t = 1.0$ and $h_T = 0.25$ [37], which falls in the stable region both in modes III and II in the 2-D case. This shows that the stability behaviour of the BIEM scheme in 2-D does not automatically translate to the equivalent 3-D case. Interestingly, in their numerical examples, instability built up in the mode II direction first, which is in conformity with the implication from our 2-D results.

7. VARIABLE TIME STEPS

As mentioned earlier, the time-step interval need not be fixed in our time-marching scheme. To illustrate the use of variable time steps, a planar 2-D crack in mode III was made to propagate bilaterally under the same condition as in Figure 1. The discrete time-step increments Δt were made to oscillate as exponential sine, with h_T varying between 0.25 and 1.0 with a period of 40 time steps. The time collocation parameter e_t was fixed at 1.0, and this choice of control parameters allowed the scheme to stay within the stability domain in Figure 5. The BIE was solved either under the explicit or implicit regime depending on the CFL criterion. Figure 10 demonstrates the good performance of this variable time step scheme. It should be noted, however, that the use of variable time-step intervals precludes the time-translation invariance of the discretized convolution kernels, thus significantly increasing the numerical expense.

8. CONCLUSION

We have presented a numerical method, based on a BIEM theory, for modelling the dynamics of a flat 2-D crack in all modes of fracture. This method has the advantage that the coefficients

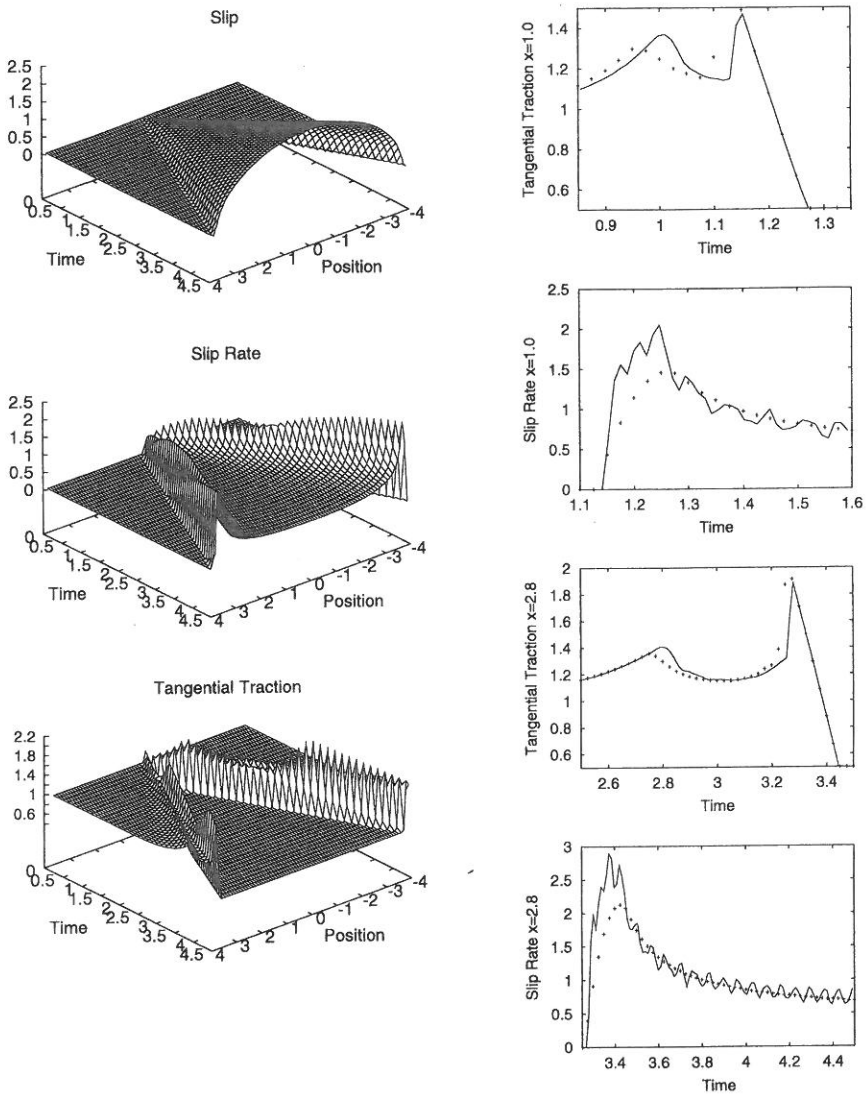

Figure 9. Self-similar mode II crack, with $h_T = 1.0$ and $e_t = 2.0$ (ε-scheme), over 180 time steps. Legends as in Figure 2a. The solid lines in the panels on the right-hand side are corresponding FDM results by Andrews and Ben-Zion [27].

in the discrete equations can be obtained in an analytical way under certain assumptions and, if the time-step interval is sufficiently small with respect to the spatial grid size, the equations simplify and can be solved explicitly. Although this method is not new for the flat 2-D anti-plane and the flat 3-D cracks, we extended it to the case of the flat 2-D in-plane crack. We have also shown that this method can be extended to the calculation of the elastic wave field off the crack plane.

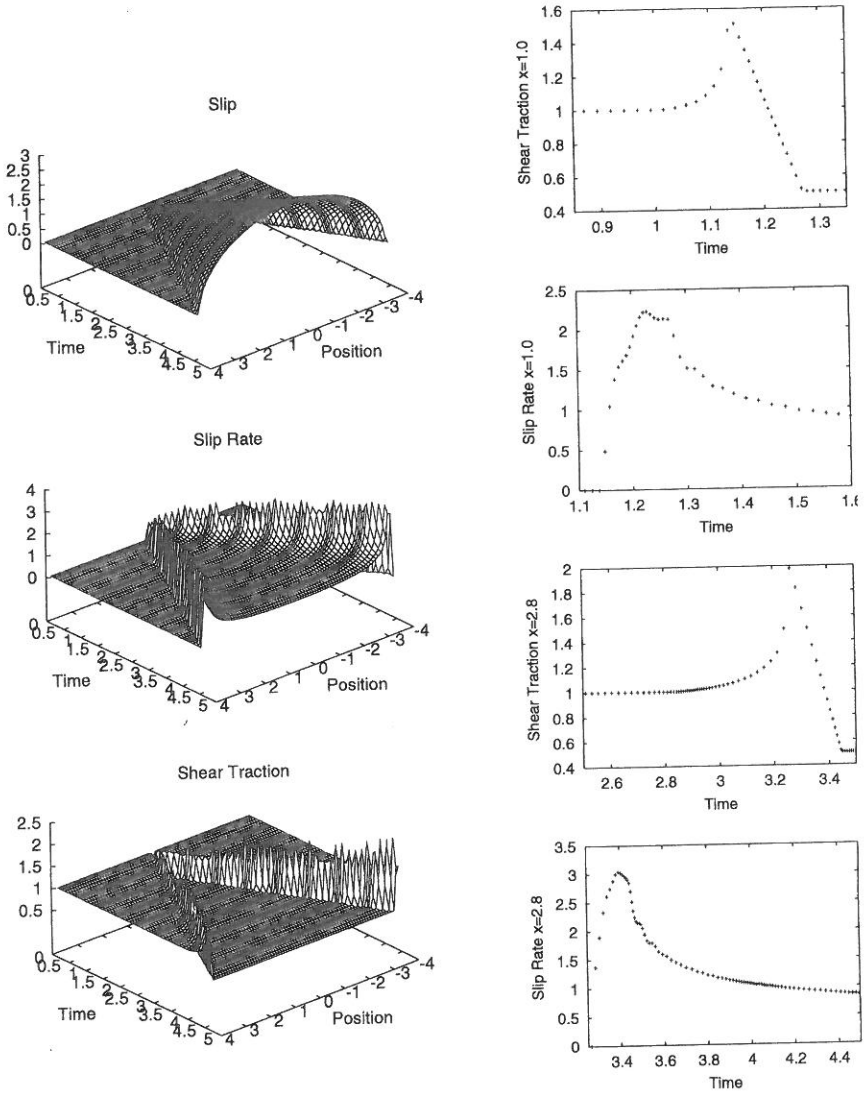

Figure 10. Self-similar mode III crack over 320 time steps of an undulating interval, with h_T oscillating between 0.25 and 1.0 and $e_t = 1.0$. Legends as in Figure 1a.

We have investigated, by means of exhaustive trial runs with different sets of control parameters, a necessary condition for the stability of this numerical scheme for all modes of fracture. It was shown that, for the case investigated, the scheme was very stable for a fairly wide range of parameters in modes I and III, and for some narrow ranges in mode II. This indicates that the numerical instabilities, pointed out by so many authors previously, may not be intrinsic to the method but depend on the choice of control parameters. The use of Peirce and Siebrits' ε-scheme [22] helped to stabilize the numerical calculation. Our method also allows for the use of variable time-step intervals.

APPENDIX. CONVOLUTION COEFFICIENTS FOR THE OFF-FAULT ELASTIC FIELD

Here we give the convolution coefficients for the discrete expressions of the off-fault stress and displacement field (29)–(32). The coefficients for the stress are

$$K^{i,j,k,n,m}_{3:\sigma 3\alpha} \equiv I_{3:\sigma 3\alpha}\left(x_1^i - s_k + \tfrac{1}{2}\Delta s, x_2^j, t_n - t_m^{\text{short}}\right) - I_{3:\sigma 3\alpha}\left(x_1^i - s_k - \tfrac{1}{2}\Delta s, x_2^j, t_n - t_m^{\text{short}}\right)$$
$$- I_{3:\sigma 3\alpha}\left(x_1^i - s_k + \tfrac{1}{2}\Delta s, x_2^j, t_n - t_m^{\text{long}}\right) + I_{3:\sigma 3\alpha}\left(x_1^i - s_k - \tfrac{1}{2}\Delta s, x_2^j, t_n - t_m^{\text{long}}\right) \quad \text{(A1)}$$

and likewise for $K^{i,j,k,n,m}_{\gamma:\sigma\alpha\beta}$, and

$$I_{3:\sigma 31}(\mathbf{x},t) = -\frac{x_2}{\pi r} H\left(t - \frac{r}{c_T}\right)\sqrt{(c_T t/r)^2 - 1} \quad \text{(A2)}$$

$$I_{3:\sigma 32}(\mathbf{x},t) = H(x_1)H\left(t - \frac{|x_2|}{c_T}\right) + \frac{1}{\pi}\operatorname{sgn}(x_1)H\left(t - \frac{r}{c_T}\right)\left[\frac{|x_1|}{r}\sqrt{(c_T t/r)^2 - 1} - \operatorname{Arccos}\frac{|x_1|}{c_T u_T}\right] \quad \text{(A3)}$$

$$I_{1:\sigma 11}(\mathbf{x},t)$$
$$= -\frac{1}{\pi}H\left(t - \frac{r}{c_L}\right)\frac{2x_2}{r}p\left\{\frac{2(3x_1^2 - x_2^2)}{3r^2}p^2\left[(c_L t/r)^2 - 1\right]^{3/2} + \left(1 - \frac{2x_2^2}{r^2}p^2\right)\sqrt{(c_L t/r)^2 - 1}\right\}$$
$$+ \frac{1}{\pi}H\left(t - \frac{r}{c_T}\right)\frac{2x_2}{r}\left\{\frac{2(3x_1^2 - x_2^2)}{3r^2}\left[(c_T t/r)^2 - 1\right]^{3/2} + \left(1 - \frac{2x_2^2}{r^2}\right)\sqrt{(c_T t/r)^2 - 1}\right\} \quad \text{(A4)}$$

$$I_{1:\sigma 22}(\mathbf{x},t)$$
$$= \frac{1}{\pi}H\left(t - \frac{r}{c_L}\right)\frac{2x_2}{r}p\left\{\frac{2(3x_1^2 - x_2^2)}{3r^2}p^2\left[(c_L t/r)^2 - 1\right]^{3/2} + \left(\frac{2x_1^2}{r^2}p^2 - 1\right)\sqrt{(c_L t/r)^2 - 1}\right\}$$
$$- \frac{1}{\pi}H\left(t - \frac{r}{c_T}\right)\frac{2x_2}{r}\left\{\frac{2(3x_1^2 - x_2^2)}{3r^2}[(c_T t/r)^2 - 1]^{3/2} + \left(\frac{2x_1^2}{r^2} - 1\right)\sqrt{(c_T t/r)^2 - 1}\right\} \quad \text{(A5)}$$

$$I_{1:\sigma 12}(\mathbf{x},t) = H(x_1)H\left(t - \frac{|x_2|}{c_T}\right)$$
$$- \frac{1}{\pi}\operatorname{sgn}(x_1)H\left(t - \frac{r}{c_L}\right)\frac{2|x_1|}{r}p\left\{\frac{2(3x_2^2 - x_1^2)}{3r^2}p^2\left[(c_L t/r)^2 - 1\right]^{3/2} + \frac{2x_2^2}{r^2}p^2\sqrt{(c_L t/r)^2 - 1}\right\}$$

$$+\frac{1}{\pi}\operatorname{sgn}(x_1)H\left(t-\frac{r}{c_T}\right)\left[\frac{2|x_1|}{r}\left\{\frac{2(3x_2^2-x_1^2)}{3r^2}\left[(c_Tt/r)^2-1\right]^{3/2}+\frac{2x_2^2}{r^2}\sqrt{(c_Tt/r)^2-1}\right\}-\operatorname{Arccos}\frac{|x_1|}{c_Tu_T}\right] \tag{A6}$$

$$\begin{aligned}I_{2:\sigma 11}(\mathbf{x},t)&=\frac{1-2p^2}{p}H(x_1)H\left(t-\frac{|x_2|}{c_L}\right)\\&-\frac{1}{\pi}\operatorname{sgn}(x_1)H\left(t-\frac{r}{c_L}\right)\left[\frac{2|x_1|}{r}p\left\{\frac{2(3x_2^2-x_1^2)}{3r^2}p^2\left[(c_Lt/r)^2-1\right]^{3/2}+\frac{2x_2^2}{r^2}p^2\sqrt{(c_Lt/r)^2-1}\right\}\right.\\&\left.+\frac{1-2p^2}{p}\operatorname{Arccos}\frac{|x_1|}{c_Lu_L}\right]\\&+\frac{1}{\pi}\operatorname{sgn}(x_1)H\left(t-\frac{r}{c_T}\right)\frac{2|x_1|}{r}\left\{\frac{2(3x_2^2-x_1^2)}{3r^2}\left[(c_Tt/r)^2-1\right]^{3/2}+\frac{2x_2^2}{r^2}\sqrt{(c_Tt/r)^2-1}\right\}\end{aligned} \tag{A7}$$

$$\begin{aligned}I_{2:\sigma 22}(\mathbf{x},t)=&\frac{1}{p}H(x_1)H\left(t-\frac{|x_2|}{c_L}\right)+\frac{1}{\pi}\operatorname{sgn}(x_1)H\left(t-\frac{r}{c_L}\right)\\&\times\left[\frac{2|x_1|}{r}p\left\{\frac{2(3x_2^2-x_1^2)}{3r^2}p^2[(c_Lt/r)^2-1]^{3/2}+2\left(1-\frac{x_1^2}{r^2}p^2\right)\sqrt{(c_Lt/r)^2-1}\right\}\right.\\&\left.-\frac{1}{p}\operatorname{Arccos}\frac{|x_1|}{c_Lu_L}\right]-\frac{1}{\pi}\operatorname{sgn}(x_1)H\left(t-\frac{r}{c_T}\right)\frac{2|x_1|}{r}\left\{\frac{2(3x_2^2-x_1^2)}{3r^2}\left[(c_Tt/r)^2-1\right]^{3/2}\right.\\&\left.+2\left(1-\frac{x_1^2}{r^2}\right)\sqrt{(c_Tt/r)^2-1}\right\}\end{aligned} \tag{A8}$$

$$I_{2:\sigma 12}(\mathbf{x},t)=I_{1:\sigma 22}(\mathbf{x},t) \tag{A9}$$

where

$$r\equiv\sqrt{x_1^2+x_2^2} \tag{A10}$$

$$u_T\equiv\sqrt{t^2-(x_2/c_T)^2} \tag{A11}$$

$$u_L\equiv\sqrt{t^2-(x_2/c_L)^2} \tag{A12}$$

In the limit $x_2\to 0$ and $x_1\to s$, (A3), (A6) and (A8) reduce to $I_{3:T3}$ in (9), $I_{1:T1}$ in (17) and $I_{2:T2}$ in (18), respectively.

The coefficients for the displacement are

$$K_{3:u3}^{i,j,k,n,m} \equiv I_{3:u3}\left(x_1^i - s_k + \tfrac{1}{2}\Delta s, x_2^j, t_n - t_m^{\text{short}}\right) - I_{3:u3}\left(x_1^i - s_k - \tfrac{1}{2}\Delta s, x_2^j, t_n - t_m^{\text{short}}\right)$$
$$- I_{3:u3}\left(x_1^i - s_k + \tfrac{1}{2}\Delta s, x_2^j, t_n - t_m^{\text{long}}\right) + I_{3:u3}\left(x_1^i - s_k - \tfrac{1}{2}\Delta s, x_2^j, t_n - t_m^{\text{long}}\right) \quad \text{(A13)}$$

and likewise for $K_{\beta:u\alpha}^{i,j,k,n,m}$, and

$$I_{3:u3}(\mathbf{x},t) = \operatorname{sgn}(x_2)H(x_1)H\left(t - \frac{|x_2|}{c_T}\right)\frac{1}{2}\left(t - \frac{|x_2|}{c_T}\right)$$
$$- \operatorname{sgn}(x_1)\operatorname{sgn}(x_2)H\left(t - \frac{r}{c_T}\right)\frac{1}{2\pi}\left(t \operatorname{Arccos}\frac{|x_1|t}{ru_T} - \frac{|x_2|}{c_T}\operatorname{Arccos}\frac{|x_1|}{c_T u_T}\right) \quad \text{(A14)}$$

$$I_{1:u1}(\mathbf{x},t) = -\frac{c_T^2 x_1 x_2}{3\pi r^4}\left\{H\left(t - \frac{r}{c_L}\right)\left[t^2 - (r/c_L)^2\right]^{3/2} - H\left(t - \frac{r}{c_T}\right)\left[t^2 - (r/c_T)^2\right]^{3/2}\right\}$$
$$+ \operatorname{sgn}(x_2)H(x_1)H\left(t - \frac{|x_2|}{c_T}\right)\frac{1}{2}\left(t - \frac{|x_2|}{c_T}\right)$$
$$- \operatorname{sgn}(x_1)\operatorname{sgn}(x_2)H\left(t - \frac{r}{c_T}\right)\frac{1}{2\pi}\left(t \operatorname{Arccos}\frac{|x_1|t}{ru_T} - \frac{|x_2|}{c_T}\operatorname{Arccos}\frac{|x_1|}{c_T u_T}\right) \quad \text{(A15)}$$

$$I_{1:u2}(\mathbf{x},t) = \frac{c_T^2(x_1^2 - x_2^2)}{6\pi r^4}\left\{H\left(t - \frac{r}{c_L}\right)\left[t^2 - (r/c_L)^2\right]^{3/2} - H\left(t - \frac{r}{c_T}\right)\left[t^2 - (r/c_T)^2\right]^{3/2}\right\}$$
$$+ \frac{1}{2\pi}H\left(t - \frac{r}{c_L}\right)p^2\sqrt{t^2 - (r/c_L)^2} + \frac{t}{4\pi}H\left(t - \frac{r}{c_L}\right)p^2 \log\frac{t - \sqrt{t^2 - (r/c_L)^2}}{t + \sqrt{t^2 - (r/c_L)^2}} \quad \text{(A16)}$$

$$I_{2:u1}(\mathbf{x},t) = \frac{c_T^2(x_1^2 - x_2^2)}{6\pi r^4}\left\{H\left(t - \frac{r}{c_L}\right)\left[t^2 - (r/c_L)^2\right]^{3/2} - H\left(t - \frac{r}{c_T}\right)\left[t^2 - (r/c_T)^2\right]^{3/2}\right\}$$
$$+ \frac{1}{2\pi}\left[H\left(t - \frac{r}{c_L}\right)(1 - p^2)\sqrt{t^2 - (r/c_L)^2} - H\left(t - \frac{r}{c_T}\right)\sqrt{t^2 - (r/c_T)^2}\right]$$
$$+ \frac{t}{4\pi}\left[H\left(t - \frac{r}{c_L}\right)(1 - p^2)\log\frac{t - \sqrt{t^2 - (r/c_L)^2}}{t + \sqrt{t^2 - (r/c_L)^2}}\right.$$
$$\left. - H\left(t - \frac{r}{c_T}\right)\log\frac{t - \sqrt{t^2 - (r/c_T)^2}}{t + \sqrt{t^2 - (r/c_T)^2}}\right] \quad \text{(A17)}$$

$$I_{2:u2}(\mathbf{x},t)=\frac{c_T^2x_1x_2}{3\pi r^4}\left\{H\left(t-\frac{r}{c_L}\right)\left[t^2-(r/c_L)^2\right]^{3/2}-H\left(t-\frac{r}{c_T}\right)\left[t^2-(r/c_T)^2\right]^{3/2}\right\}$$
$$+\operatorname{sgn}(x_2)H(x_1)H\left(t-\frac{|x_2|}{c_L}\right)\frac{1}{2}\left(t-\frac{|x_2|}{c_L}\right)$$
$$-\operatorname{sgn}(x_1)\operatorname{sgn}(x_2)H\left(t-\frac{r}{c_L}\right)\frac{1}{2\pi}\left(t\operatorname{Arccos}\frac{|x_1|t}{ru_L}-\frac{|x_2|}{c_L}\operatorname{Arccos}\frac{|x_1|}{c_Lu_L}\right) \quad \text{(A18)}$$

Their time derivatives are given by

$$\dot{I}_{3:u3}(\mathbf{x},t)=\operatorname{sgn}(x_2)H(x_1)H\left(t-\frac{|x_2|}{c_T}\right)\frac{1}{2}-\operatorname{sgn}(x_1)\operatorname{sgn}(x_2)H\left(t-\frac{r}{c_T}\right)\frac{1}{2\pi}\operatorname{Arccos}\frac{|x_1|t}{ru_T} \quad \text{(A19)}$$

$$\dot{I}_{1:u1}(\mathbf{x},t)=-\frac{c_T^2x_1x_2t}{\pi r^4}\left[H\left(t-\frac{r}{c_L}\right)\sqrt{t^2-(r/c_L)^2}-H\left(t-\frac{r}{c_T}\right)\sqrt{t^2-(r/c_T)^2}\right]$$
$$+\operatorname{sgn}(x_2)H(x_1)H\left(t-\frac{|x_2|}{c_T}\right)\frac{1}{2}-\operatorname{sgn}(x_1)\operatorname{sgn}(x_2)H\left(t-\frac{r}{c_T}\right)\frac{1}{2\pi}\operatorname{Arccos}\frac{|x_1|t}{ru_T} \quad \text{(A20)}$$

$$\dot{I}_{1:u2}(\mathbf{x},t)=\frac{c_T^2(x_1^2-x_2^2)t}{2\pi r^4}\left[H\left(t-\frac{r}{c_L}\right)\sqrt{t^2-(r/c_L)^2}-H\left(t-\frac{r}{c_T}\right)\sqrt{t^2-(r/c_T)^2}\right]$$
$$+\frac{1}{4\pi}H\left(t-\frac{r}{c_L}\right)p^2\log\frac{t-\sqrt{t^2-(r/c_L)^2}}{t+\sqrt{t^2-(r/c_L)^2}} \quad \text{(A21)}$$

$$\dot{I}_{2:u1}(\mathbf{x},t)=\frac{c_T^2(x_1^2-x_2^2)t}{2\pi r^4}\left[H\left(t-\frac{r}{c_L}\right)\sqrt{t^2-(r/c_L)^2}-H\left(t-\frac{r}{c_T}\right)\sqrt{t^2-(r/c_T)^2}\right]$$
$$+\frac{1}{4\pi}\left[H\left(t-\frac{r}{c_L}\right)(1-p^2)\log\frac{t-\sqrt{t^2-(r/c_L)^2}}{t+\sqrt{t^2-(r/c_L)^2}}\right.$$
$$\left.-H\left(t-\frac{r}{c_T}\right)\log\frac{t-\sqrt{t^2-(r/c_T)^2}}{t+\sqrt{t^2-(r/c_T)^2}}\right] \quad \text{(A22)}$$

$$\dot{I}_{2:u2}(\mathbf{x},t)=\frac{c_T^2x_1x_2t}{\pi r^4}\left[H\left(t-\frac{r}{c_L}\right)\sqrt{t^2-(r/c_L)^2}-H\left(t-\frac{r}{c_T}\right)\sqrt{t^2-(r/c_T)^2}\right]$$
$$+\operatorname{sgn}(x_2)H(x_1)H\left(t-\frac{|x_2|}{c_L}\right)\frac{1}{2}-\operatorname{sgn}(x_1)\operatorname{sgn}(x_2)H\left(t-\frac{r}{c_L}\right)\frac{1}{2\pi}\operatorname{Arccos}\frac{|x_1|t}{ru_L} \quad \text{(A23)}$$

As $x_2\to 0$ and $x_1\to s$, (A14), (A15) and (A18) reduce to

$$I_{3:u3}=I_{1:u1}=I_{2:u2}=\frac{t}{2}\operatorname{sgn}(x_2)H(t)H(s) \quad \text{(A24)}$$

ACKNOWLEDGEMENTS

The authors benefitted from discussions with D. J. Andrews, Hideo Aochi, Alain Cochard, Shamita Das, Attilio Frangi, Eiichi Fukuyama, Nobuki Kame, James R. Rice, Thomas Seelig and Teruo Yamashita, as well as from comments by two anonymous referees. Part of this work was done while one of the authors (TT) stayed at the École Normale Supérieure on a Postdoctoral Fellowship for Research Abroad of the Japan Society for the Promotion of Science (JSPS).

REFERENCES

1. Beskos DE. Boundary element methods in dynamic analysis: Part II (1986–1996). *Applied Mechanics Reviews* 1997; **50**:149–197.
2. Zhang Ch. A novel derivation of non-hypersingular time-domain BIEs for transient elastodynamic crack analysis. *International Journal of Solids and Structures* 1991; **28**:267–281.
3. Cochard A, Madariaga R. Dynamic faulting under rate-dependent friction. *Pure and Applied Geophysics* 1994; **142**:419–445.
4. Cochard A, Madariaga R. Complexity of seismicity due to highly rate-dependent friction. *Journal of Geophysical Research* 1996; **101**:25321–25336.
5. Zhang Ch, Gross D. A non-hypersingular time-domain BIEM for 3-D transient elastodynamic crack analysis. *International Journal for Numerical Methods in Engineering* 1993; **36**:2997–3017.
6. Fukuyama E, Madariaga R. Integral equation method for plane crack with arbitrary shape in 3D elastic medium. *Bulletin of the Seismological Society of America* 1995; **85**:614–628.
7. Fukuyama E, Madariaga R. Rupture dynamics of a planar fault in a 3D elastic medium: rate- and slip-weakening friction. *Bulletin of the Seismological Society of America* 1998; **88**:1–17.
8. Koller MG, Bonnet M, Madariaga R. Modelling of dynamical crack propagation using time-domain boundary integral equations. *Wave Motion* 1992; **16**:339–366.
9. Siebrits E, Crouch SL. Two-dimensional elastodynamic displacement discontinuity method. *International Journal for Numerical Methods in Engineering* 1994; **37**:3229–3250.
10. Tada T, Yamashita T. Non-hypersingular boundary integral equations for two-dimensional non-planar crack analysis. *Geophysical Journal International* 1997; **130**:269–282.
11. Seelig Th, Gross D. Analysis of dynamic crack propagation using a time-domain boundary integral equation method. *International Journal of Solids and Structures* 1997; **34**:2087–2103.
12. Seelig Th, Gross D. On the interaction and branching of fast running cracks—a numerical investigation. *Journal of the Mechanics and Physics of Solids* 1999; **47**:935–952.
13. Seelig Th, Gross D. On the stress wave induced curving of fast running cracks—a numerical study by a time-domain boundary element method. *Acta Mechanica* 1999; **132**:47–61.
14. Tada T, Fukuyama E, Madariaga R. Non-hypersingular boundary integral equations for 3-D non-planar crack dynamics. *Computational Mechanics* 2000; **25**:613–626.
15. Aochi H. Theoretical studies on dynamic rupture propagation along a 3D non-planar fault system. *Doctor of Science Thesis*, The University of Tokyo, Tokyo, 1999.
16. Aochi H, Fukuyama E, Matsu'ura M. Spontaneous rupture propagation on a non-planar fault in 3D elastic medium. *Pure and Applied Geophysics* 2000; in press.
17. Perrin G, Rice JR, Zheng G. Self-healing slip pulse on a frictional surface. *Journal of the Mechanics and Physics of Solids* 1995; **43**:1461–1495.
18. Geubelle PH, Rice JR. A spectral method for three-dimensional elastodynamic fracture problems. *Journal of the Mechanics and Physics of Solids* 1995; **43**:1791–1824.
19. Cochard A, Rice JR. A spectral method for numerical elastodynamic fracture analysis without spatial replication of the rupture event. *Journal of the Mechanics and Physics of Solids* 1997; **45**:1393–1418.
20. Ravi-Chandar K, Yang B. On the role of microcracks in the dynamic fracture of brittle materials. *Journal of the Mechanics and Physics of Solids* 1997; **45**:535–563.
21. Das S, Kostrov BV. On the numerical boundary integral equation method for three-dimensional dynamic shear crack analysis. *Transactions of the ASME Journal of Applied Mechanics* 1987; **54**:99–104.
22. Peirce A, Siebrits E. Stability analysis of model problems for elastodynamic boundary element discretizations. *Numerical Methods for Partial Differential Equations* 1996; **12**:585–613.
23. Peirce A, Siebrits E. Stability analysis and design of time-stepping schemes for general elastodynamic boundary element models. *International Journal for Numerical Methods in Engineering* 1997; **40**:319–342.
24. Ida Y. Cohesive force across the tip of a longitudinal-shear crack and Griffith's specific surface energy. *Journal of Geophysical Research* 1972; **77**:3796–3805.
25. Das S, Aki K. A numerical study of two-dimensional spontaneous rupture propagation. *Geophysical Journal of the Royal Astronomical Society* 1977; **50**:643–668.

26. Andrews DJ. Dynamic growth of mixed-mode shear cracks. *Bulletin of the Seismological Society of America* 1994; **84**:1184–1198.
27. Andrews DJ, Ben-Zion Y. Wrinkle-like slip pulse on a fault between different materials. *Journal of Geophysical Research* 1997; **102**:553–571.
28. Madariaga R, Olsen K, Archuleta R. Modeling dynamic rupture in a 3D earthquake fault model. *Bulletin of the Seismological Society of America* 1998; **88**:1182–1197.
29. Bécache E. A variational boundary integral equation method for an elastodynamic antiplane crack. *International Journal for Numerical Methods in Engineering* 1993; **36**:969–984.
30. Schanz M, Antes H. Application of 'Operational Quadrature Methods' in time domain boundary element methods. *Meccanica* 1997; **32**:179–186.
31. Rice JR. Spatio-temporal complexity of slip on a fault. *Journal of Geophysical Research* 1993; **98**:9885–9907.
32. Frangi A, Novati G. On the numerical stability of time-domain elastodynamic analyses by BEM. *Computer Methods in Applied Mechanics and Engineering* 1999; **173**:403–417.
33. Frangi A. Elastodynamics by BEM: a new direct formulation. *International Journal for Numerical Methods in Engineering* 1999; **45**:721–740.
34. Frangi A. 'Causal' shape functions in the time domain boundary element method. *Computational Mechanics* 2000; **25**:533–541.
35. Lubich Ch. On the multistep time discretization of linear initial-boundary value problems and their boundary integral equations. *Numerische Mathematik* 1994; **67**:365–389.
36. Birgisson B, Siebrits E, Peirce AP. Elastodynamic direct boundary element methods with enhanced numerical stability properties. *International Journal for Numerical Methods in Engineering* 1999; **46**:871–888.
37. Madariaga R, Fukuyama E. Rupture dynamics of a planar fault in 3D studied by a boundary integral equation method (abstract). *International Symposium on Boundary Element Methods, Symposium Proceedings*, Paris, 1998; 129–130.